

COHERENT NEUTRAL CURRENT NEUTRINO-NUCLEUS SCATTERING AT A SPALLATION SOURCE; A VALUABLE EXPERIMENTAL PROBE

J.D. Vergados^{1,2}, F.T. Avignone III³ and I. Giomataris⁴

⁽¹⁾*University of Ioannina, Ioannina, GR 45110, Greece .*

⁽²⁾*Theory Division, CERN, CH,*

⁽³⁾*University of South Carolina, Columbia, SC 29208, USA, and*

⁽⁴⁾*CEA, Saclay, DAPNIA, Gif-sur-Yvette, Cedex, France,*

(Dated: October 30, 2018)

The coherent contribution of all neutrons in neutrino nucleus scattering due to the neutral current is examined considering the Spallation Neutron Source (SNS) as a source of neutrinos. SNS is a prolific pulsed source of electron and muon neutrinos as well as muon antineutrinos.

PACS numbers: 13.15.+g, 14.60Lm, 14.60Bq, 23.40.-s, 95.55.Vj, 12.15.-y.

INTRODUCTION

The question of detecting and exploiting neutrinos from both terrestrial and extra terrestrial sources has become central to physics and astrophysics. In recent years, in particular, exploiting the neutral current interaction for detecting neutrino induced nuclear recoils has become fashionable. Indeed due to the coherence of all neutrons in the nucleus one gets very large cross sections, which are proportional to the square of the neutron number (the coherent neutral current contribution due to protons is negligible). To exploit this feature, however, one should design large detectors with very low energy thresholds. Two possibilities have been considered:

- Spherical TPC detectors filled with a noble gas for supernova neutrino detection. Such detectors can give us information about the neutrino source, since the neutral current interaction is not sensitive to detailed neutrino properties like neutrino masses, mixing etc, which appear in neutrino oscillations. It has also been pointed out that such detectors are robust, cheap and easy to maintain for years. So they can surely detect supernovae at distances of tens of kiloparsecs [1].
- The standard direct dark matter detectors aim at detecting nuclear recoils due to WIMP's (weakly interacting massive particles). Since the expected event rates are extremely low, one may have to worry about the rare background recoils due to neutrino sources, like the solar ⁸B neutrinos [2], [3].

It is thus important to study the behavior of such detectors using well known terrestrial neutrino sources. One such source is Spallation Neutron Source (SNS) at the Oak Ridge National Laboratory, Oak Ridge, Tennessee, which is the most powerful source of pulsed intermediate-energy neutrinos [4],[5].

The primary parameters of the SNS are as follows:

Proton beam power on target: 1.4 MW

Proton beam kinetic energy: 1.0 GeV.

Average beam current on target: 1.4 mA

Protons per pulse on target: 1.5×10^{14}

Pulse repetition rate: 60 Hz

π^+ per proton: 0.068

π^+ per second 6.14×10^{14}

$R(\nu_e) = R(\bar{\nu}_\mu) = 6.14 \times 10^{14}$

The total neutrino flux at a distance r is:

$$\Phi(\nu_e, r) = \Phi(\bar{\nu}_\mu, r) = \Phi(\nu_\mu, r) = \frac{6.14 \times 10^{14} \text{s}^{-1}}{4\pi r^2} \quad (1)$$

At a typical distance of 50 m we find:

$$\Phi(\nu_e, r) = \Phi(\bar{\nu}_\mu, r) = \Phi(\nu_\mu, r) = 1.95 \times 10^6 \text{ cm}^{-2} \text{ s}^{-1} \quad (2)$$

The normalized neutrino spectra can be described very well by the shapes exhibited in Fig. 1

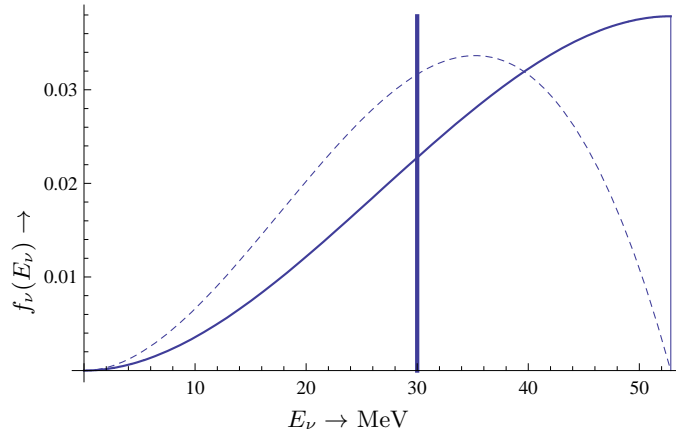


FIG. 1: The neutrino spectrum from stopped pions. The normalized dashed and solid curves correspond to ν_e and $\bar{\nu}_\mu$ respectively. Also shown is the discrete ν_μ spectrum (thick vertical line).

ELASTIC NEUTRINO NUCLEON SCATTERING

The cross section for elastic neutrino nucleon scattering has extensively been studied. It has been shown that at low energies it can be simplified and be cast in the form: [6],[7]:

$$\begin{aligned} \left(\frac{d\sigma}{dT_N} \right)_{weak} &= \frac{G_F^2 m_N}{2\pi} [(g_V + g_A)^2 \\ &+ (g_V - g_A)^2 \left[1 - \frac{T_N}{E_\nu}\right]^2 + (g_A^2 - g_V^2) \frac{m_N T_N}{E_\nu^2}] \end{aligned} \quad (3)$$

where m_N is the nucleon mass, T_N its energy and g_V, g_A are the weak coupling constants. Neglecting their dependence on the momentum transfer to the nucleon they take the form:

$$g_V = -2 \sin^2 \theta_W + 1/2 \approx 0.04, \quad g_A = \frac{1.27}{2}, \quad (\nu, p) \quad (4)$$

$$g_V = -1/2, \quad g_A = -\frac{1.27}{2}, \quad (\nu, n) \quad (5)$$

In the above expressions for the axial current the renormalization in going from the quark to the nucleon level was taken into account. For antineutrinos $g_A \rightarrow -g_A$. To set the scale we write:

$$\frac{G_F^2 m_N}{2\pi} = 5.14 \times 10^{-41} \frac{\text{cm}^2}{\text{MeV}} \quad (6)$$

The nucleon energy depends on the neutrino energy and the scattering angle, the angle between the direction of the recoiling particle and that of the incident neutrino. In the laboratory frame it is given by:

$$T_N = \frac{2 m_N (E_\nu \cos \theta)^2}{(m_N + E_\nu)^2 - (E_\nu \cos \theta)^2}, \quad 0 \leq \theta \leq \pi/2 \quad (7)$$

(forward scattering). For sufficiently small neutrino energies, the last equation can be simplified as follows:

$$T_N \approx \frac{2(E_\nu \cos \theta)^2}{m_N}$$

The above formula can be generalized to any target and can be written in dimensionless form as follows:

$$y = \frac{2 \cos^2 \theta}{(1 + 1/x_\nu)^2 - \cos^2 \theta} \quad , \quad y = \frac{T_{recoil}}{m_{recoil}} \quad , \quad x_\nu = \frac{E_\nu}{m_{recoil}} \quad (8)$$

In the present calculation we will treat x_ν and y as dynamical variables, in line with CDM recoils. One, of course, equally well could have chosen x_ν and θ as relevant variables.

The maximum energy occurs when $\theta = 0$, i.e.:

$$y_{max} = \frac{2}{(1 + 1/x_\nu)^2 - 1} \quad (9)$$

in agreement with Eq. (2.5) of ref. [6]. One can invert Eq. 8 and get the neutrino energy associated with a given recoil energy and scattering angle. One finds

$$x_\nu = \left[-1 + \cos \theta \sqrt{1 + \frac{2}{y}} \right]^{-1} \quad , \quad 0 \leq \theta \leq \pi/2 \quad (10)$$

The minimum neutrino energy for a given recoil energy is given by:

$$x_\nu^{min} = \left[-1 + \sqrt{1 + \frac{2}{y}} \right]^{-1} = \frac{y}{2} \left(1 + \sqrt{1 + \frac{2}{y}} \right) \quad (11)$$

in agreement with Eq. (4.2) of ref. [6]. The last equation is useful in obtaining the differential cross section (with respect to the recoil energy) after folding with the neutrino spectrum

COHERENT NEUTRINO NUCLEUS SCATTERING

From the above expressions we see that the vector current contribution, which may lead to coherence, is negligible in the case of the protons. Thus the coherent contribution [8] may come from the neutrons and is expected to be proportional to the square of the neutron number. The neutrino-nucleus scattering can be derived in analogous fashion. It can also be obtained from the amplitude of the neutrino nucleon scattering by employing the appropriate kinematics, i.e. those involving the elastically scattered nucleus and the substitution

$$\mathbf{q} \Rightarrow \frac{\mathbf{p}}{A} \quad , \quad E_N \Rightarrow \sqrt{m_N^2 + \frac{\mathbf{p}^2}{A^2}} = \frac{E_A}{A}$$

with \mathbf{q} the nucleon momentum, A is the nuclear mass number and \mathbf{p} the nuclear momentum. Under the above assumptions the neutrino-nucleus cross section takes the form:

$$\begin{aligned} \left(\frac{d\sigma}{dT_A} \right) &= \frac{G_F^2 A m_N}{2\pi} [(M_V + M_A)^2 \left(1 + \frac{T_A}{E_\nu} \right) \\ &+ (M_V - M_A)^2 \left(1 - \frac{T_A}{E_\nu} \right)^2 + (M_A^2 - M_V^2) \frac{A m_N T_A}{E_\nu^2}] \end{aligned} \quad (12)$$

where M_V and M_A are the nuclear matrix elements associated with the vector and the axial currents respectively and T_A is the energy of the recoiling nucleus. The axial current contribution vanishes

for $0^+ \Rightarrow 0^+$ transitions. Anyway, it is negligible in the case of coherent scattering on neutrons. Thus Eq. (12) is reduced to:

$$\left(\frac{d\sigma}{dT_A}\right)_{weak} = \frac{G_F^2 A m_N}{2\pi} (N^2/4) F_{coh}(T_A, E_\nu), \quad (13)$$

with

$$F_{coh}(T_A, E_\nu) = F^2(q^2) \left(1 + \left(1 - \frac{T_A}{E_\nu}\right)^2 - \frac{A m_N T_A}{E_\nu^2}\right) \quad (14)$$

where N is the neutron number and $F(q^2) = F(T_A^2 + 2A m_N T_A)$ is the nuclear form factor. The effect of the nuclear form factor depends on the target, since the maximum recoil energy depends on the target (see Fig. 2).

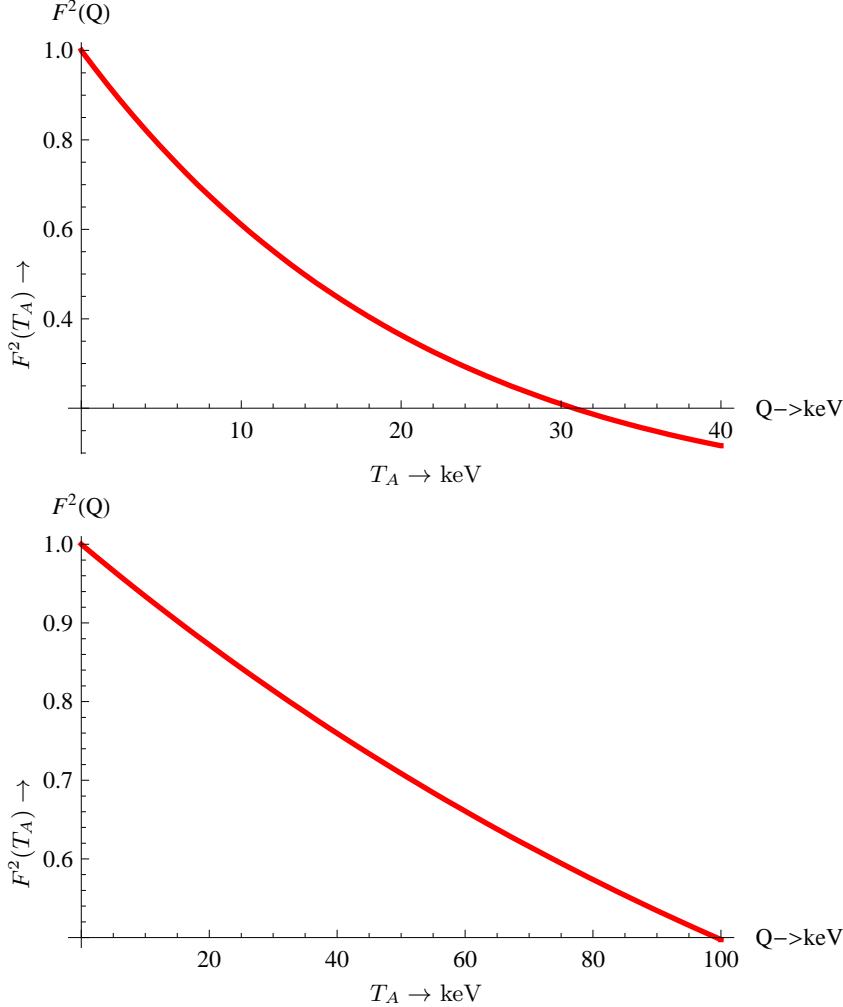


FIG. 2: The square of the nuclear form factor, $F^2(T_A)$, as a function of the recoil energy for $A=131$ (top) and $A=40$ (bottom). Note that the maximum recoil energy is different for each target.

QUENCHING FACTORS AND ENERGY THRESHOLDS

. The above results refer to an ideal detector operating down to zero energy threshold. For a real detector, however, as we have already mentioned, the nuclear recoil events are quenched, especially

at low energies. The quenching factor for a given detector is the ratio of the signal height for a recoil track divided by that of an electron signal with the same energy. We should not forget that the signal heights depend on the velocity and how the signals are extracted experimentally. The actual quenching factors must be determined experimentally for each target. In the case of NaI the quenching factor is 0.05, while for Ge and Si it is 0.2-0.3. For our purposes it is adequate, to multiply the energy scale by an recoil energy dependent quenching factor, $Q_{fac}(T_A)$ adequately described by the Lidhard theory [9]. More specifically in our estimate of $Qu(T_A)$ we assumed a quenching factor of the following empirical form [9], [10]:

$$Q_{fac}(T_A) = r_1 \left[\frac{T_A}{1keV} \right]^{r_2}, \quad r_1 \simeq 0.256, \quad r_2 \simeq 0.153 \quad (15)$$

The quenching factors very much depend on the detector type. The quenching factor, exhibited in

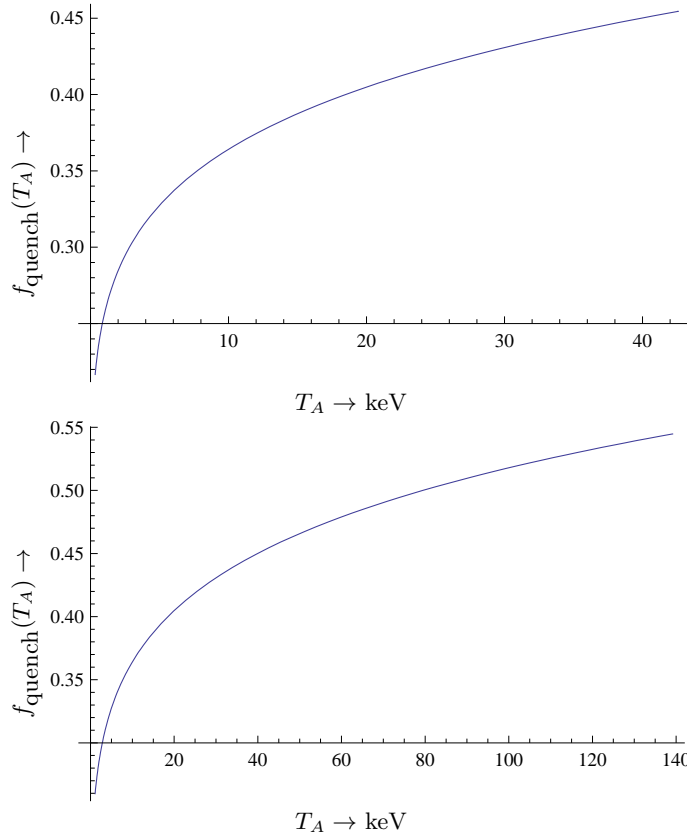


FIG. 3: The quenching factor as a function of the recoil energy in the case of $A=131$ (top) and $A=40$ (bottom).

Fig. 3 for recoil energies of ^{131}Xe and ^{40}Ar , were obtained assuming the same quenching of the form of Eq. (15). In the presence of the quenching factor as given by Eq. (15) the measured recoil energy is typically reduced by factors of about 3, when compared with the electron energy. In other words a threshold energy of electrons of 1 keV becomes 3 keV for nuclear recoils.

RESULTS

For a heavy target, ^{131}Xe

The neutrino-nucleus cross sections are shown in Figs 4 and 5. The quenching factor does not affect the rate (see Figs 4 and 5) but it shifts the threshold downwards. In other words the unavailable phase space is on the left of the thin line with no quenching and the thick line with quenching. Clearly the effect of quenching is going to be larger when the recoil energy is smaller. Integrating

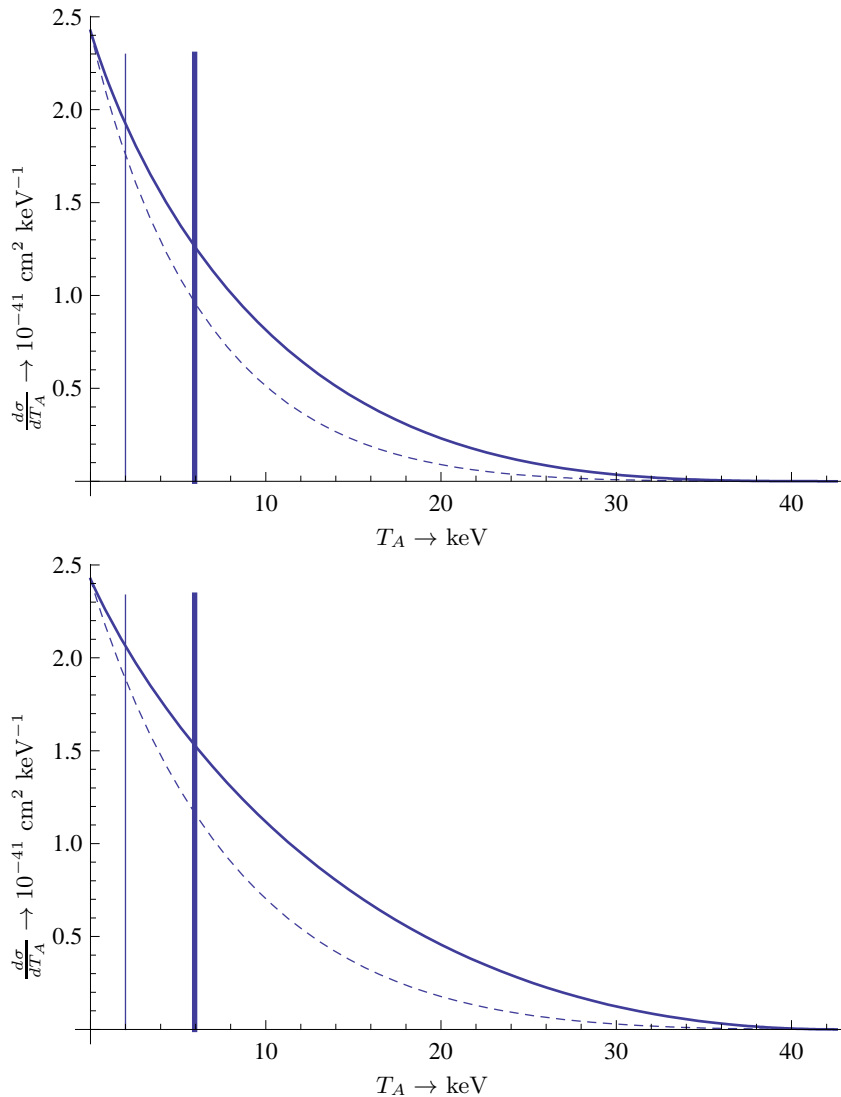


FIG. 4: The differential neutrino nucleus cross section as a function of the recoil energy in the case of $A=131$ for the continuous ν_e spectrum (top) and the continuous $\bar{\nu}_\mu$ spectrum (bottom). The solid (dashed) curves correspond to no form factor (form factor) respectively. The fine vertical line corresponds to a threshold of 3 keV. The phase space on its left is unavailable. Due to the presence of quenching the excluded phase space becomes larger (on the left of the thick line).

the differential rates shown Figs 4 and 5 at zero threshold we obtain the total rates shown in table I. The effect of a non zero threshold is exhibited in Figs 6 and 7. It is clear that both the effect of the inclusion of the form factor and of quenching are important, especially in the case of high energy threshold, but the effect of quenching is most important of the two.

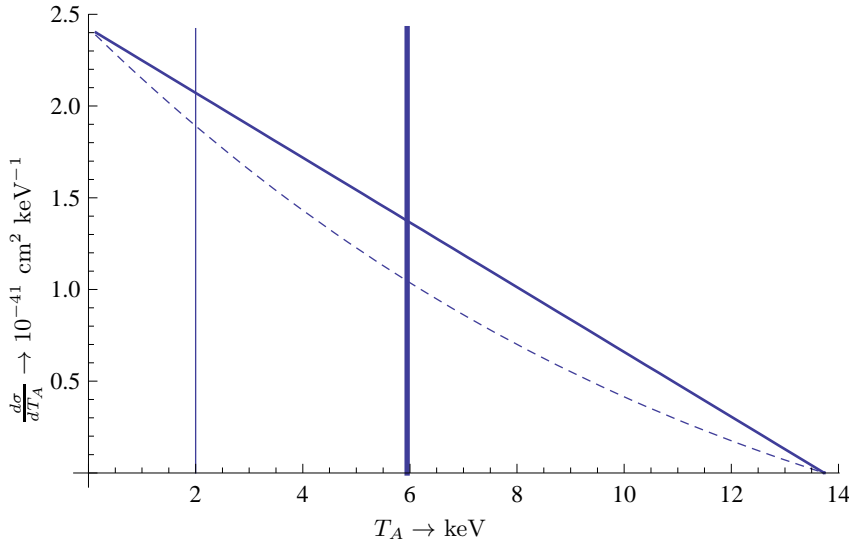


FIG. 5: The same as in Fig. 4 for the discrete ν_μ spectrum.

TABLE I: The neutrino-nucleus total cross section in units of 10^{-41}cm^{-2} due to the neutral current

target	ν_e (no FF)	ν_e (FF)	$\bar{\nu}_\mu$ (no FF)	$\bar{\nu}_\mu$ (FF)	ν_μ (no FF)	ν_μ (FF)
^{131}Xe	2.71	1.98	3.60	2.46	2.79	1.79
^{40}Ar	0.221	0.190	0.294	0.244	0.178	0.162

For a light target, ^{40}Ar

The differential cross sections are now shown in Figs 8 and 9. Integrating the differential rates shown Figs 8 and 9 at zero threshold we obtain the total rates shown in table II. The effect of a non zero threshold is exhibited in Figs 10 and 11. The effect of quenching now is less dramatic since the recoil energy for a light target is higher. The total number of events for a target of mass m in time t is given by

$$R = 3.156 \times 10^7 \frac{m_t}{1kg} \frac{t}{1y} \Phi(\nu, L) \sigma(\nu, (A, N)) \frac{1000}{A_t} N_A \quad (16)$$

where $N_A = 6.02 \times 10^{23}$ is Avogadro's number, A_t the mass number of the target, $\sigma(\nu, (A, N))$ is the coherent neutrino-nucleus cross section and $\Phi(\nu, L)$ is the neutrino flux (neutrinos per second per cm^2) in distance L from the source. Using

$$\Phi(\nu, L = 50\text{m}) = 1.96 \times 10^6 \text{cm}^{-2}\text{s}^{-1}$$

for each flavor we obtain the data of table II.

EXPERIMENTAL ISSUES WITH THE SPHERICAL TPC

The SNS facility provides an excellent opportunity to employ and test the spherical TPC gaseous detector [11] of volume V under pressure P and temperature T filled with a noble gas. This detector

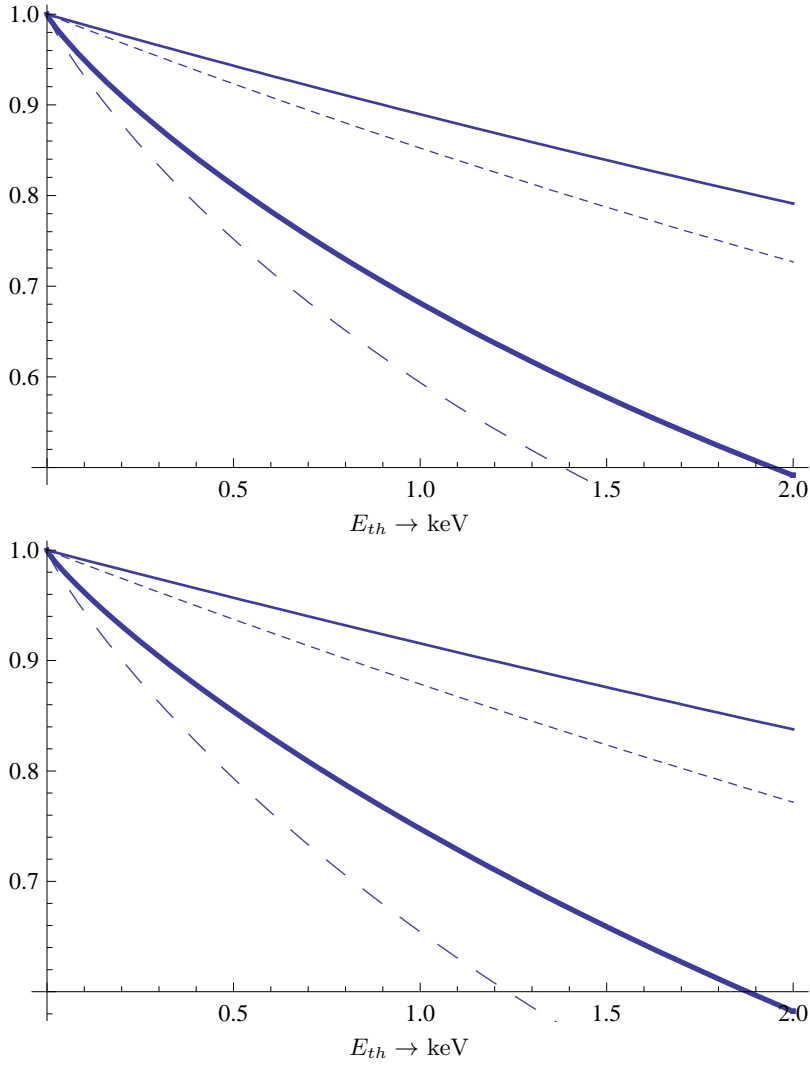


FIG. 6: The event rates at a given energy threshold divided by the corresponding ones at zero threshold as a function of the threshold energy in the case of $A=131$ target for the continuous ν_e spectrum (top) and the continuous $\bar{\nu}_\mu$ spectrum (bottom). The solid (dashed) curves correspond to no form factor (form factor) respectively. The two lowest curves take into account to the quenching factor.

has good resolution and very low energy threshold. In this case we obtain:

$$R = 3.156 \times 10^7 \frac{t}{1y} \Phi(\nu, L) \sigma(\nu, (A, N)) \frac{PV}{kT} s(L, x)$$

where the parameter $s(L, x)$ depends on the shape of the vessel and the distance L of its center from the source. Using

$$\Phi(\nu, L = 50\text{m}) = 1.96 \times 10^6 \text{cm}^{-2}\text{s}^{-1}$$

for each flavor we obtain the data of table III. The function $s(L, x)$ for a sphere of radius R with its center at a distance L from the source is given by

$$s(R, R/L) = \frac{L^2}{(4/3)\pi R^3} 2\pi \int_{L-R}^{L+R} r^2 dr \int_0^\pi d\theta \sin \theta \frac{1}{R^2 + r^2 + 2rL \cos \theta} \quad (17)$$

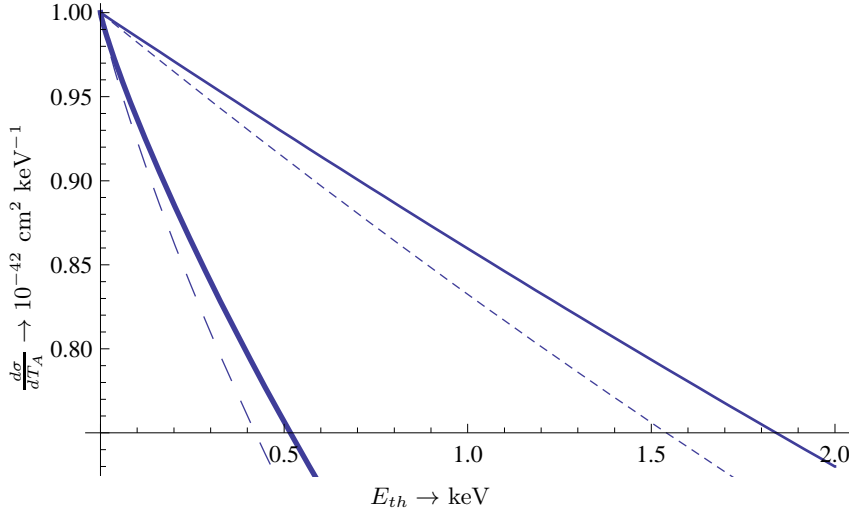


FIG. 7: The same as in Fig. 6 for the discrete ν_μ spectrum.

TABLE II: The event rates for nuclear recoils per ton per year due to neutral current neutrino-nucleus scattering for a detector at a distance $L=50\text{m}$ away from the neutrino source with zero energy threshold.

target	ν_e (no FF)	ν_e (FF)	$\bar{\nu}_\mu$ (no FF)	$\bar{\nu}_\mu$ (FF)	ν_μ (no FF)	ν_μ (FF)	all ν (no FF)	all ν (FF)
^{131}Xe	7.70	5.64	10.3	6.99	6.21	5.09	24.0	17.69
^{40}Ar	2.06	1.77	2.74	2.27	1.66	1.51	6.46	5.5

The ratio $s(R, R/L)/s(10, 0.2)$ is shown in Fig. 12. The experimental set up is shown in Fig. 13. Using an appropriate field corrector the field inside the detector is spherically symmetric (see Fig. 14).

DISCUSSION AND CONCLUSIONS

The total number of events per ton-y at 50 m is:

$$R(\text{Xe}) = 17.8(\text{events per ton-y}), \quad R(\text{Ar}) = 5.5(\text{events per ton-y}) \quad (18)$$

One notices the following:

1. The content of tables II-III can be understood by comparing it to other neutrino sources. The flux at 50 m is $\Phi = 3\Phi_{\bar{\nu}_e} = 5.85 \times 10^6 \text{cm}^{-2}\text{s}^{-1}$. This is comparable to that of solar boron neutrinos $\Phi_{\nu_e} = 5.0 \times 10^6 \text{cm}^{-2}\text{s}^{-1}$, but with a higher cross section, since the latter is characterized by lower average energy. Thus the relatively low flux and energy of the boron solar neutrinos cannot cause any background problems to dark matter searches [2]. Anyway the number of neutrinos in a year is $N_\nu = 1.8 \times 10^{14} \text{cm}^{-2}$. The corresponding quantities for supernovae neutrinos at a distance $D = 3.1 \times 10^{22} \text{cm}$, are [1] $\Phi_{\nu_e} = 1.5 \times 10^{12} \text{cm}^{-2}$, $\Phi_{\bar{\nu}_e} = 1.0 \times 10^{12} \text{cm}^{-2}$ and $\Phi_{\nu_\alpha} = 6.3 \times 10^{11} \text{cm}^{-2}$ for all other flavors α , i.e a total of $3.1 \times 10^{12} \text{cm}^{-2}$. In other words, since the energy spectra are not very different, the event rate here is expected to be higher than that of a typical supernova in our galaxy[1].
2. The event rate per unit target mass predicted does not favor the heavy target according to

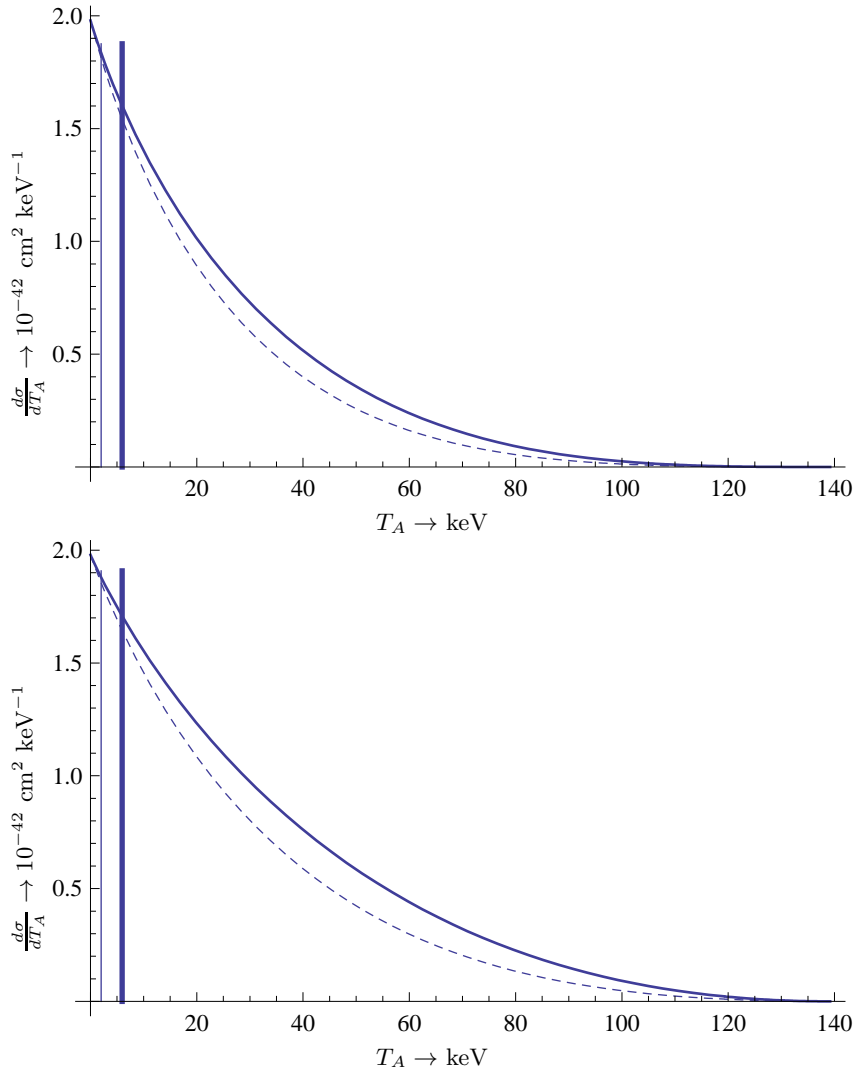


FIG. 8: The differential neutrino nucleus cross section as a function of the recoil energy in the case of $A=40$ for the continuous ν_e spectrum (top) and the continuous $\bar{\nu}_\mu$ spectrum (bottom). The solid (dashed) curves correspond to no form factor (form factor) respectively. The fine vertical line corresponds to a threshold of 3 keV. The phase space on its left is unavailable. Due to the presence of quenching the excluded phase space becomes larger (on the left of the thick line).

the expected N^2 rule implied by the differential cross section (compare Figs 4-5 and 8-9) for the following reasons:

- There fewer atoms in a kg of a heavy target. So one expects:

$$R \propto \frac{N^2}{A}.$$

- The phase space available favors a light target, since, for a given neutrino energy, the nuclear recoil energy decreases with A . This kinematical advantage maybe partly offset by the fact that the effect of form factor becomes more important, if the recoil energy becomes higher.
- Threshold effects may somewhat complicate the issue (compare Figs 6-7 and 10-11).

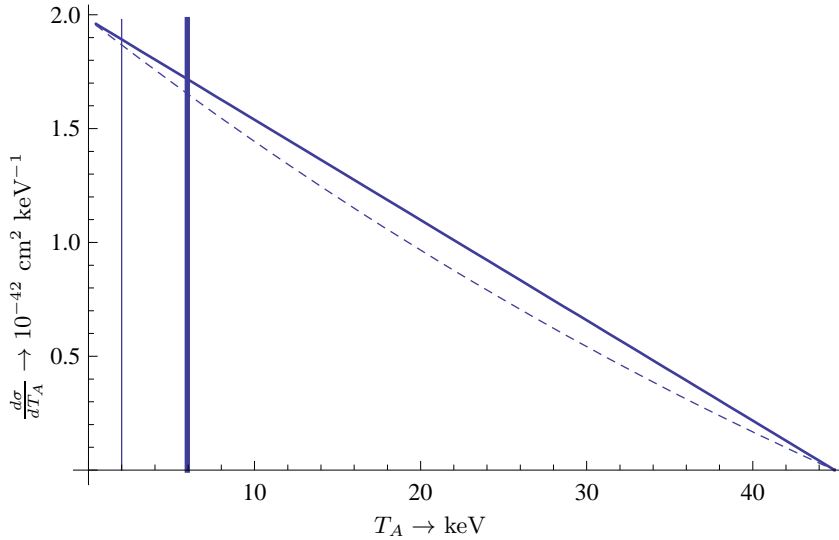


FIG. 9: The same as in Fig. 8 for the discreet ν_μ spectrum.

TABLE III: The event rates for nuclear recoils per year due to neutral current neutrino-nucleus scattering for a detector with the shape of a sphere of radius $R = 10$ m with its center at a distance $L = 50$ m from the source ($s(10,0.2)=1.008$). The vessel is filled with gas under pressure $P = 10$ atm and temperature $T = 300$ °K. The detector is assumed to operate at zero threshold.

target	ν_e (no FF)	ν_e (FF)	$\bar{\nu}_\mu$ (no FF)	$\bar{\nu}_\mu$ (FF)	ν_μ (no FF)	ν_μ (FF)	all ν (no FF)	all ν (FF)
^{131}Xe	1705	1249	2280	1548	1393	1120	5379	3917
^{40}Ar	139.3	119.7	185.3	153.5	112.2	102.1	436.86	375.3

This N^2 dependence clearly applies whenever the amount of the target material for a given volume is determined by the pressure (see table III) in agreement with our earlier work on supernova neutrino detectors [1].

Acknowledgments: One of the authors (JDV) is happy to acknowledge support by MRTN-CT-2006 (UniverseNet) and is indebted to the CERN Theory Division for support and hospitality during the last phases of this work. One of us (FTA) was supported by the National Science Foundation Grant PHY-0500337.

-
- [1] Y. Giomataris and J. Vergados, Phys. Lett. **B 634**, 23 (2006), ; hep-ex/0503029.
[2] J. Vergados and H. Ejiri, Nuc. Phys. **B 804**, 144 (2008), ; hep-ex/0503029.
[3] J.D. Vergados, H. Ejiri and I. Giomataris, Solar Neutrinos as Background arXiv:0809.0785.
[4] F. A. III and Y. V. Efremenko, J. Phys. G: Nuc.Part. Phys **29**, 2615 (2003); See also the SNS web site: "neutrons.ornl.gov" (Facilities/Technical Parameters).
[5] F.T. Avignone III, Private Communication.
[6] J. Beacom, W. Farr, and P. Vogel, Phys. Rev. **D 66**, 03301 (2002).
[7] P. Vogel and J. Engel, Phys. Rev. **D 39**, 3378 (1989).
[8] E.A. Paschos, A. Kartavtsev, hep-ph/0309148.
[9] J. Lidhart *et al*, Mat. Phys. Medd. Dan. Vid. Selsk, 33 (1963) 1.
[10] E. Simon, et al, Nucl. Instr. Meth. **A 507**, 643 (2003).

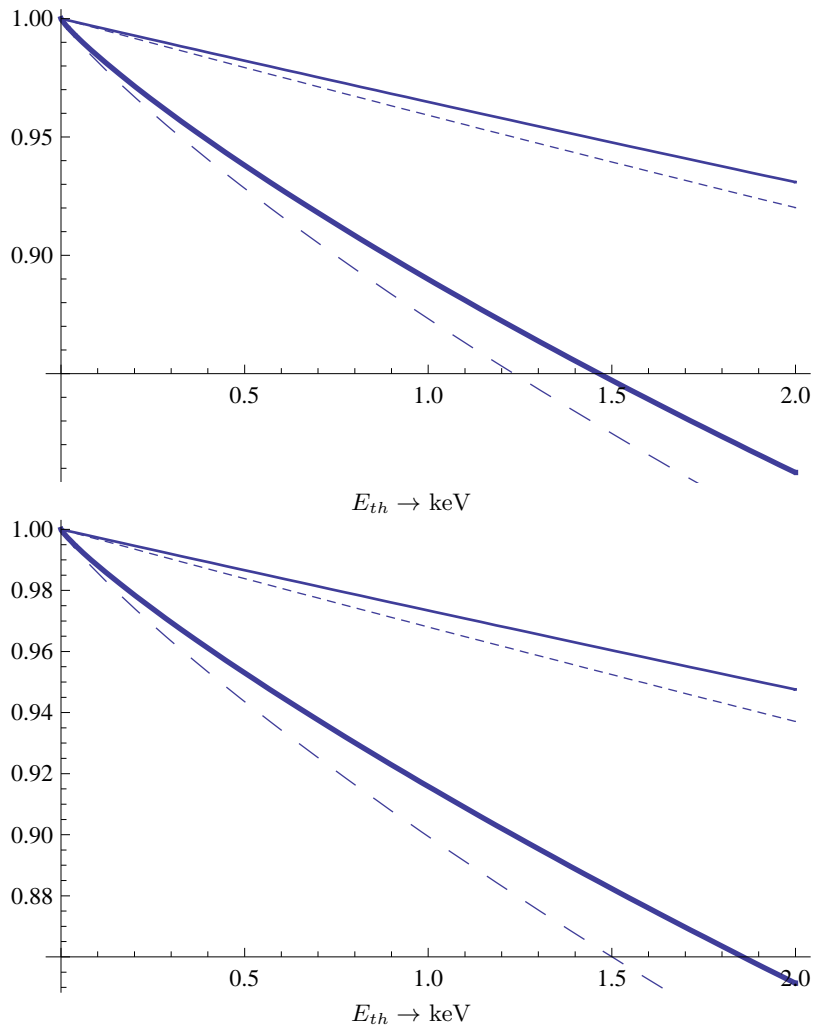


FIG. 10: The event rates at a given energy threshold divided by the corresponding ones at zero threshold as a function of the threshold energy in the case of $A=40$ target for the continuous ν_e spectrum (top) and the continuous $\bar{\nu}_\mu$ spectrum (bottom). The continuous (dashed) curves correspond to no form factor (form factor) respectively. In each figure the thick solid and the long dash curves also take into account the quenching factor.

[11] I. Giomataris, I. Irastorza, I. Savvidis, S. Andriamonje, S. Aune, M. Chapelier, P. Charvin, P. Colas, J. Derre, E. Ferrer, et al., JINST **3**, P09007 (2008), arXiv:0807.2802.

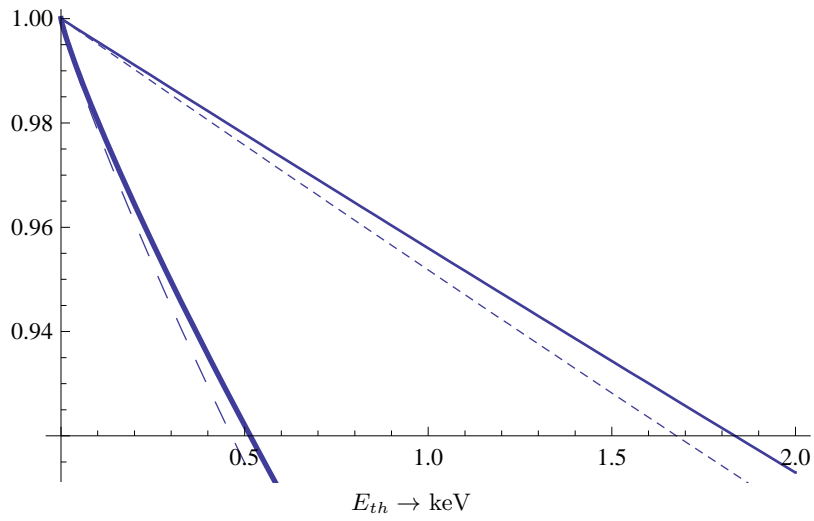


FIG. 11: The same as in Fig. 10 for the discreet ν_μ spectrum.

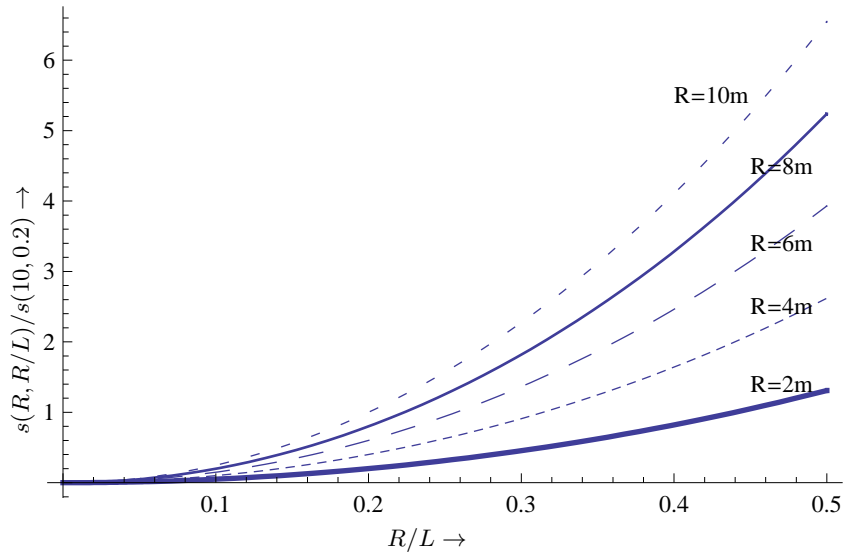


FIG. 12: The parameter $s(R, R/L)$ (see text) in the case of a sphere of radius R whose center is at a distance L from the source.

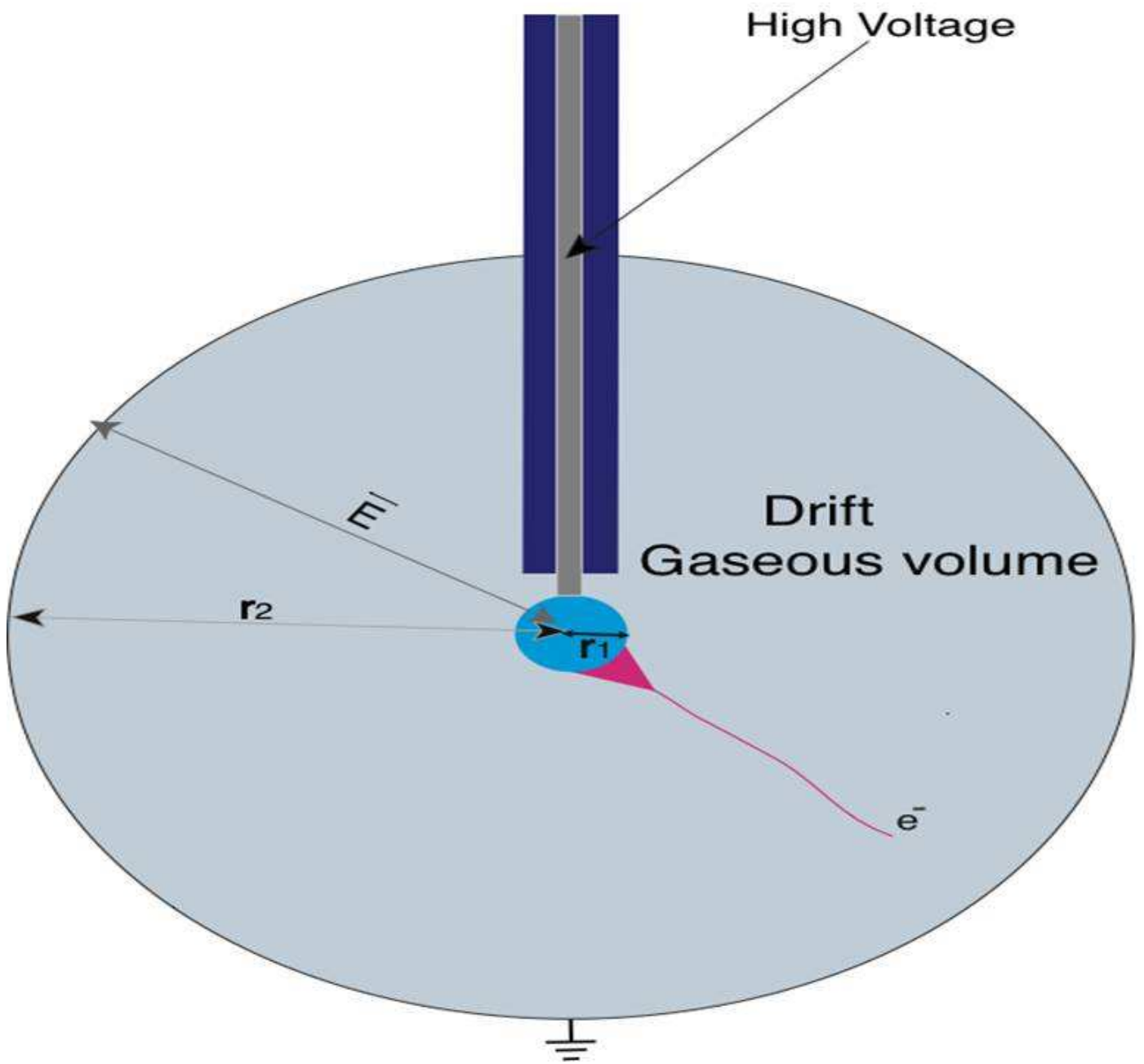


FIG. 13: A sketch of spherical TPC detector to be employed in studying the coherent scattering of neutrons employed in this work.

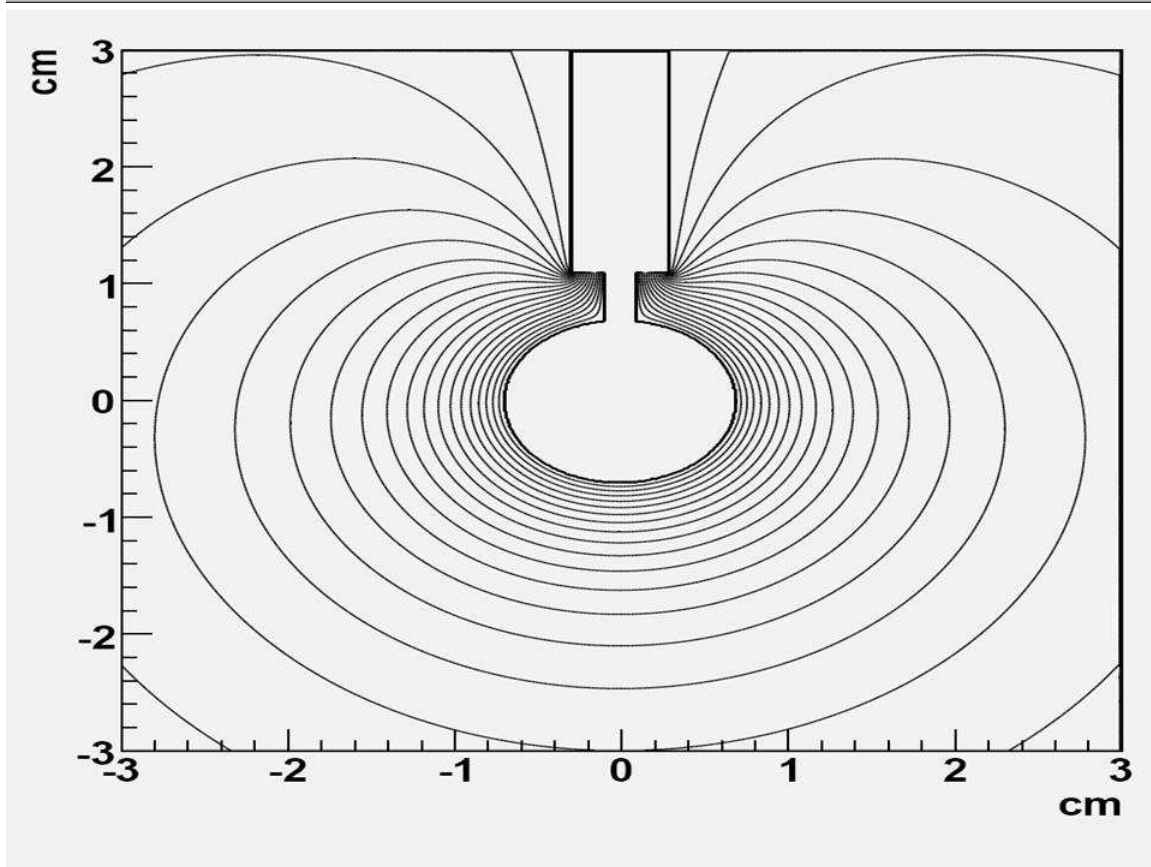
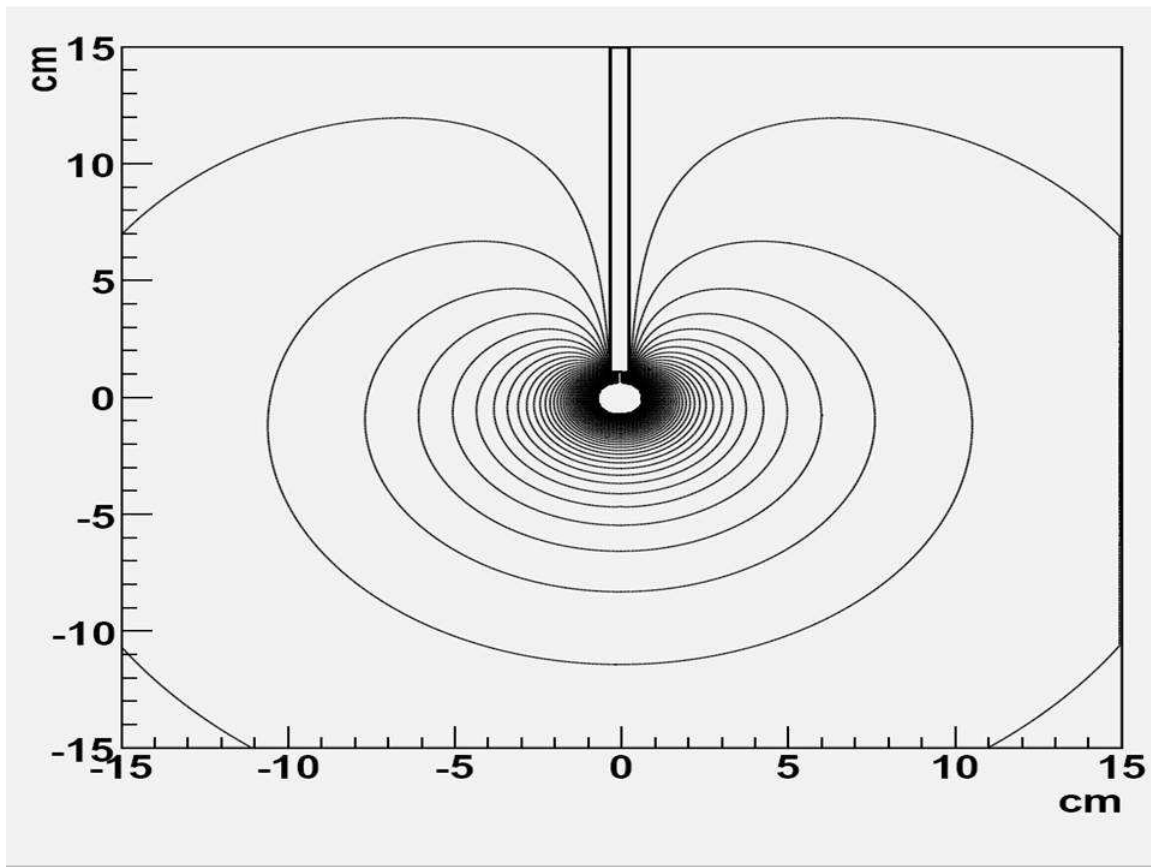


FIG. 14: The Equipotential surfaces inside the spherical vessel of Fig. 13. In spite of the wire connecting the inside and the outside spheres the field corrector introduced ensures that the electric field is spherically symmetric.